

4.2 Spatio-temporally Resolved Emission Spectroscopy of Inductive Spark Ignition in Atmospheric Air Condition

Wooyeong Kim, Choongsik Bae, Tobias Michler, Olaf Toedter,
Thomas Koch

Abstract

Current transistorized coil ignition (TCI) system consists of ignition coil and spark plug, whose electrical properties, structure and gas composition determine entire discharge processes and therefore the early stage of combustion. In this work, a new measurement and diagnostic technique were developed and tested to investigate the early phases of spark ignition process. The spark discharge of commercial TCI system was analyzed by using spatio-temporally resolved optical emission spectroscopy to find out the interrelation of the characteristic evolution of discharge with the formation of reactive species inside the activated volume.

The emission spectra of inductive spark discharge in atmospheric air were measured at the range of wavelength from 300 to 800 nm, while the secondary voltage and current of spark ignition system were acquired simultaneously. An optical probe with linearly arranged glass fiber bundle was used to achieve spatial distribution of emission intensity vertically along the electrode gap of spark plug. At the same time, the time series of emission spectra were illustrated by using the precise gate shift operation of intensified CCD camera mounted on the spectrograph.

The emission of electronically excited species such as molecular nitrogen, atomic oxygen and electrode material were effectively measured with the spectral resolution of 0.2 nm. During the abrupt increase of current in breakdown phase, only molecular nitrogen emission was exclusively detected. It was followed by the atomic oxygen and electrode material, which are closely related to the flame initiation and electrode wear respectively. The activated volume of spark discharge near cathode showed higher emission intensity for all the aforementioned species in comparison with the region near anode. The electronic, vibrational and rotational temperatures of the discharge were calculated by using additional spectra measurement at selective wavelength range with spectral resolution of 0.1 nm. Alongside the calorimetric measurement, the temperature profile over position and time allowed the quantitative evaluation of energy-transfer efficiency of spark discharge into the gas mixture.

1 Introduction

Spark ignition is a way of initiating the combustion process of fuel-air mixture by generating electrical discharge in the combustion chamber of internal combustion engine. Current spark-ignition (SI) engines for passenger cars are equipped with transistorized coil ignition (TCI) systems, which comprise of an ignition coil and a spark plug for each cylinder. The ignition coil has primary and secondary coils, which provide high-voltage electric potential between the middle and ground electrodes of spark plug. The spark ignition is apparently the most important process of SI engine operation, since the thermodynamic condition of mixture at ignition timing directly affects the fuel consumption and the pollutant emission of the engine [1].

The conventional TCI system, however, acts as a technology which limits further efficiency improvement, because the advanced combustion process results in unfavorable thermodynamic condition for igniting the fuel-air mixture. Therefore, various types of alternative ignition systems have been developed and tested while aiming at extending ignitability limit and/or reducing the burn delay. The application of non-thermal plasma has been recognized as the most promising solution in the recent decades. Nevertheless, the traditional combination of ignition coil and spark plug still remains as the only available mass-production ignition system due to its high cost-effectiveness and reliability at most of engine operation points.

Spark discharge is a phenomenon with dynamic nature, thus it accompanies sudden changes in its physical property and close-to-zero repeatability in real experiment condition. The term “spark discharge” may have to be recognized as a collective term describing a phenomenon, in which a plasma channel is generated with bright and sudden “flash” between two electrodes. In addition, the spark discharge process of automotive spark ignition system does not follow the well-known voltage-current profile of gas discharges [2], since in the case of coil ignition the charge carriers cannot be steadily provided with increasing discharge current as assumed in the gas discharge physics.

This work aimed to characterize the spark discharge process for automotive application by developing a package of diagnostic technique and analysis tool on the basis of established theory and experimental approaches in the gas discharge physics. Based on this experimental data, the sequence of reactive species formation and variation of discharge temperature were investigated and illustrated in the form of both spatially and temporally resolved information. There exist a great number of related previous studies and methodologies to be reviewed, but this literature work is instead to be properly covered in the authors' publication [3]. The essential backgrounds for the experimental approaches and data analysis are included in corresponding sections.

2 Experimental setup

2.1 Spark ignition system and electrical measurement

The spark discharge was generated between the central and ground electrodes of a commercial spark plug in atmospheric-pressure air. A commercial spark plug was mounted in a tinplate chamber, which ensures electromagnetic shielding from the surroundings. The chamber and the entire measurement devices were placed in an air-conditioned laboratory facility. A commercial ignition coil was used to provide ignition voltage to the spark plug electrodes. The discharge voltage was measured by a high-voltage probe (Tektronix P6015A), and the current was measured by a current monitor

(Pearson Electronics 2877). The measured voltage and current were acquired by a four-channel oscilloscope (LeCroy WaveRunner 6030A with bandwidth of 350 MHz) with triggered data-logging function (Figure 1).

2.2 Spectroscopic measurement

The light emission of spark discharge was transmitted through a fiber-optic cable, in which seven glass fibers are linearly arranged at both ends (Figure 2). The glass fibers have core diameter of 100 μm and numerical apparatus of 0.22. One end of the cable was located in front of the spark plug electrodes, while the 3-dimensional positioning of the cable end was adjusted by using precise optomechanical devices (Figure 3). The other end of the cable was adapted to the entrance slit of a spectrograph, so that the light was transmitted while the spatial distribution of emission can be maintained. The spectrograph (Acton Research Corporation SP-2556 with focal length of 500 mm) was equipped with three different gratings, among them the gratings with density of 1200 and 600 grooves/mm were used in the experiment. An intensified charge-coupled device (ICCD) camera (Princeton Instrument PI-MAX with full-size resolution of 1024x256 pixels) was mounted to the spectrograph to record the spectra. The gain, gate timing and gate width were programmed by the Programmable Timing Generator (PTG) module of the spectrograph. The PTG ensures a precise gate control in sub-nanosecond range.

2.3 Calibration for spectroscopic measurement

Precise calibration is necessary to minimize errors, which may arise from every part of the whole optical system. A calibration lamp using low-pressure discharge of gaseous mercury and argon (LOT-Oriel LSP035) was used for the wavelength calibration of spectrograph system and calculation of spectral resolution. The intensive atomic emission lines of mercury and argon lie from 200 to 450 nm and 700 to 800 nm respectively, thus these could cover the wavelength ranges of interest.

Besides, the luminous intensity of the ray arriving the spectrograph may be locally reduced due to the inconsistent transmittance of the optical components, especially the fiber optics in this setup. To compensate this, the transmittance of the system was also calculated by measuring the continuous emission spectra of a tungsten calibration lamp (Osram WI 17/G). Here, the absolute transmittance was not able to obtain, but the spatial distribution of relative transmittance was calculated and used in the post-processing of spectra.

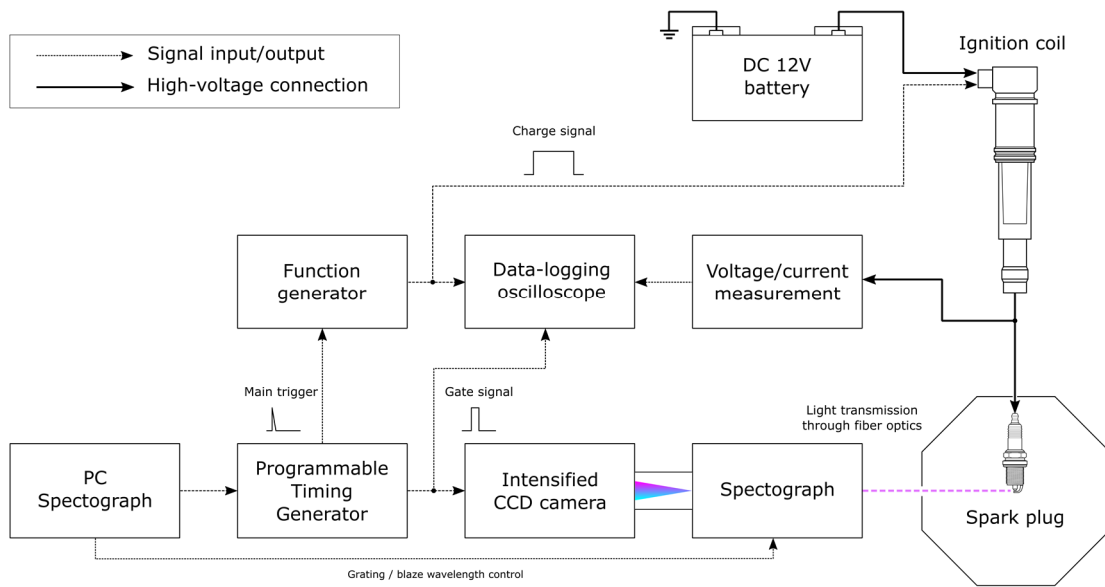


Figure 1: Schematic diagram of the experimental setup.



Figure 2: Linear bundle end of the fiber-optic cable.

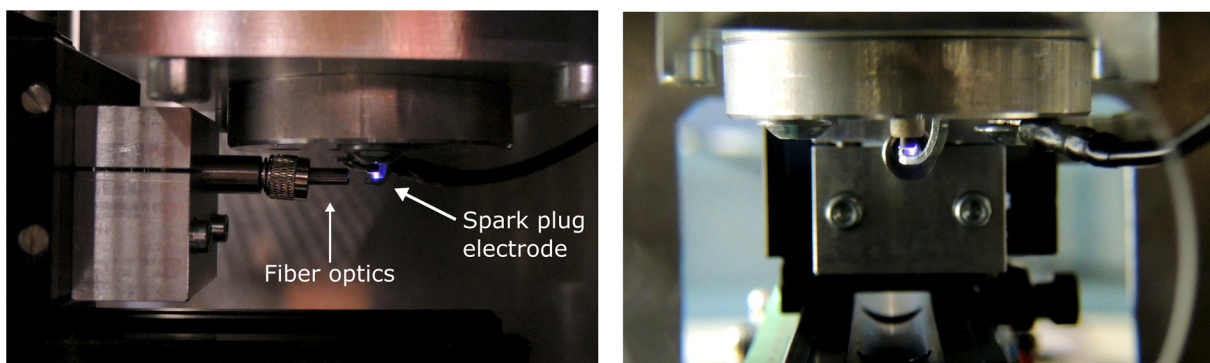


Figure 3: Configuration of spark plug and fiber optics with optomechanical components.

2.4 Signal synchronization

The test campaign was designed to be driven by automated macro process of spectrograph control system. Figure 4 schematically shows how trigger signals of the measurement system were synchronized. A measurements begins with giving start trigger

from the control PC of spectrograph to PTG. The PTG then generates a trigger to the function generator to charge the ignition coil. At the same time, another identical trigger is generated from the PTG to the oscilloscope to acquire voltage and current data from each measuring devices (probes). The PTG is also controlled by the spectrograph PC, in which the gate delay and gate width of intensified CCD camera can be controlled. The macro process is so programmed that the gate delay increases by gate width after each measurement. The gate signal for each measurement is also acquired by the oscilloscope simultaneously.

The gate timing sweep scheme is illustrated in Figure 5 with secondary voltage and current profile. The initial gate width was set to 10 μs to secure both temporal resolution and sufficient signal-to-noise ratio. After 400 μs from the breakdown (start of discharge), the gate width had to become longer up to 100 μs , since the luminous emission of the glow discharge phase was much weaker than the breakdown and arc phase. This does not actually deteriorate the temporal resolution, because obviously a rapid change in physical properties in this phase is unlikely to occur. For each time step, the measurement was repeated for ten times.

In summary, three sets of electrical data – secondary voltage, secondary current, and ICCD gate time – and one spectrum are achieved after each measurement. This synchronization scheme facilitates creating a time series of spatially-resolved spectra by arranging the spectra by each gate timing in the post-processing.

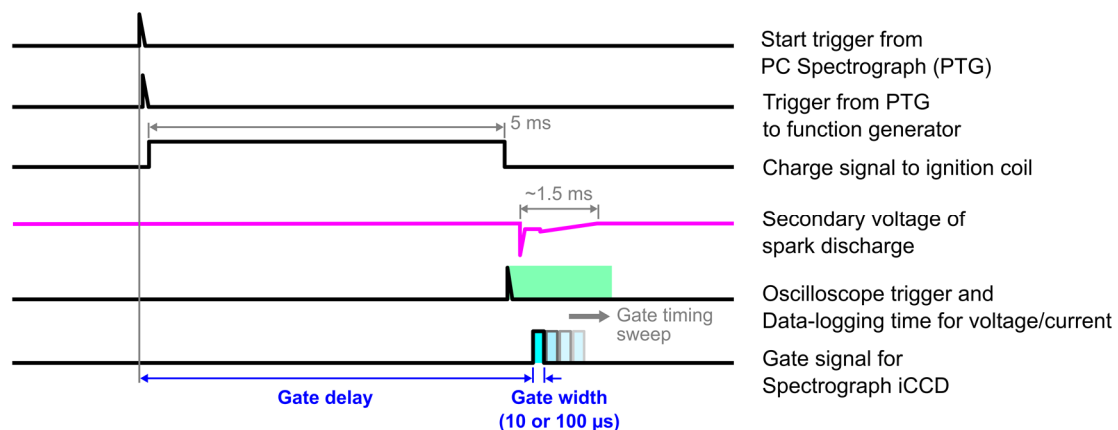


Figure 4: Synchronization of main trigger with charge signal, oscilloscope trigger and gate time for spectrum measurement (PTG: Programmable Timing Generator).

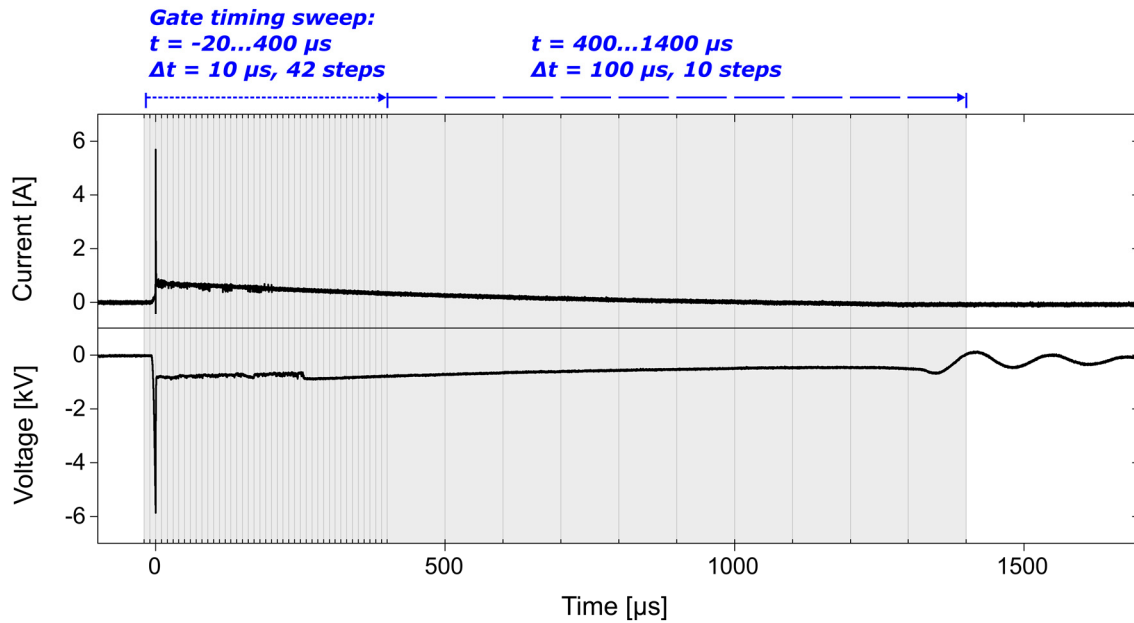


Figure 5: Gate timing sweep scheme with two different gate width.

3 Results and discussion

3.1 Time series of emission spectra

Figure 6 shows the time series of measured emission spectra of spark discharge in two wavelength ranges. In this measurement, the central wavelength was varied from 300 to 780 nm with 40 nm step by using the grating with 600 grooves/mm. In combination with the entrance slit width of 100 μm , the spectral resolution (FWHM, full width at half maximum) of measured spectra was calculated to be 0.2 nm.

Here, the spatially-distributed emission intensities were added together and mean values of ten repetition were calculated. To highlight the temporal variation in emission lines, the spectra with time step of 10 μs were merged to show the spectra variation consistently with fixed time step of 100 μs . In Figure 6, only the first spectra at $t=0$ in each diagram were measured with time step of 10 μs . Each spectrum was normalized with its gate delay to fairly compare the emission intensity.

In the whole wavelength range, the emission intensity was dramatically reduced just after the breakdown – around 90% on peak-value basis. Most of the emission peaks were easily recognizable on the basis of previous studies on atmospheric-condition air discharge [4, 5] and spectroscopic data [6, 7]. In the breakdown phase, nitrogen molecule (N_2) emitted intense light – the second positive system (C-B) between 300 and 400 nm and the first positive system (B-X) between 600 and 800 nm – with its distinct rotational-vibrational structure. As breakdown ended, the well-known atomic emission of oxygen ($\text{O } 1$) in 777 nm sharply increased. As the oxygen emission decreased gradually, relatively intense and sharp emission lines were detected for around 200 μs . These peaks between 340 and 360 nm are the atomic emission lines of nickel ($\text{Ni } 1$), which is the one of the major elements of electrodes. This time scale approximately corresponds to the conventional definition of arc discharge phase. After then, roughly in the transition towards glow discharge, the molecular ion of nitrogen (N_2^+) emission – the first negative system in 391 nm – became as intensive as the N_2 emission. After

400 μs , no sudden change in spectrum took place, and the intensity decreased globally until the end of discharge.

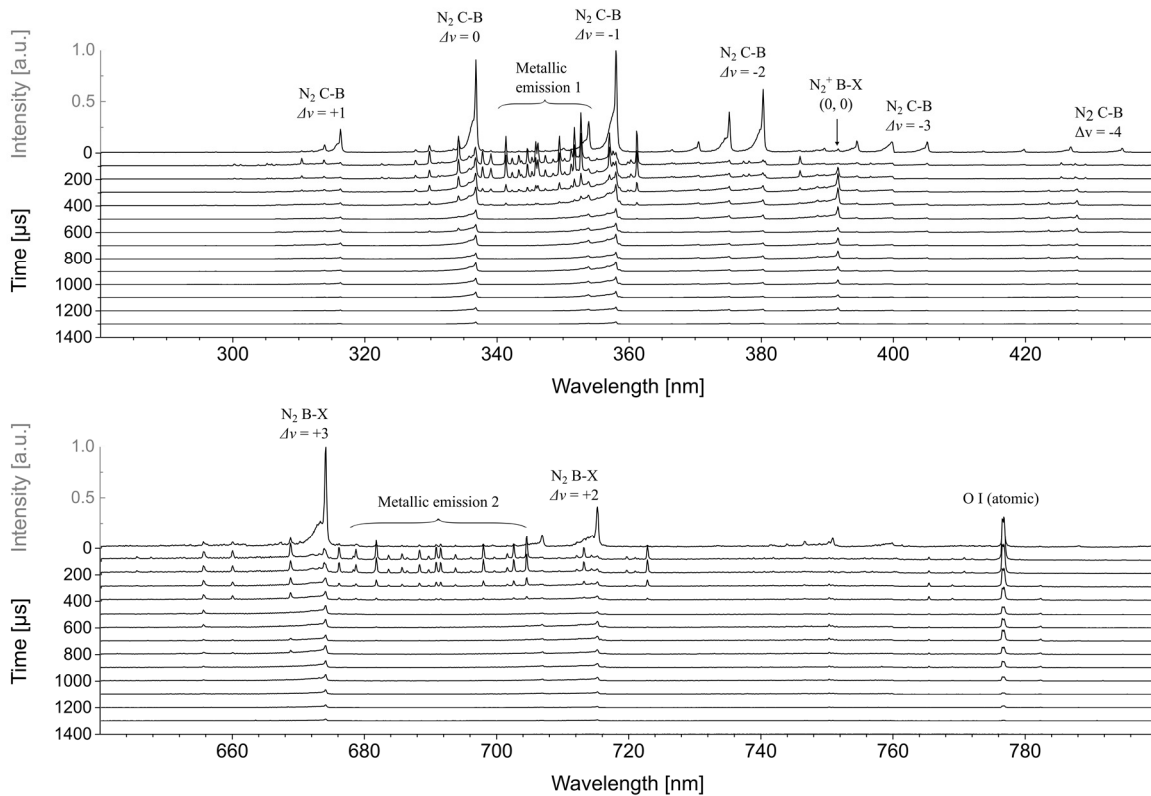


Figure 6: Time series of emission spectra of spark discharge.

3.2 Spatio-temporal distribution of reactive species formation

The measured spectra were post-processed to track the formation of reactive species within the spark discharge. Four emission peaks were selected:

- N_2 C-B (0, 0) emission at 337.0 nm,
- Ni I atomic emission at 341.4 nm,
- N_2^+ B-X (0, 0) emission at 391.2 nm, and
- O I atomic emission at 777.1 nm.

Figure 7 shows the distribution of peak intensities in color on time and position axes. Each diagram in this figure – and some of the following figures – contains seven strips of data, which represent the light emission transmitted via seven glass fibers. The “position” denoted here represents the vertical position from the ground electrode (anode), thereby the upper most strip corresponds to the closest position to the central electrode (cathode). Each data point is an averaged value of ten repetitions.

In all the four diagrams, the upper half of the region generally shows higher emission intensities than the lower half. This indicates that the formation of these species occurs more actively near the cathode than the anode. As watching the variation on the time axis, the time, in which each species formation is most active, lies side by side for the four species. Since the emission intensity represent the concentration of excited species, this result clearly identifies the dynamics of the early spark discharge process by establishing the sequence of reactive species formation.

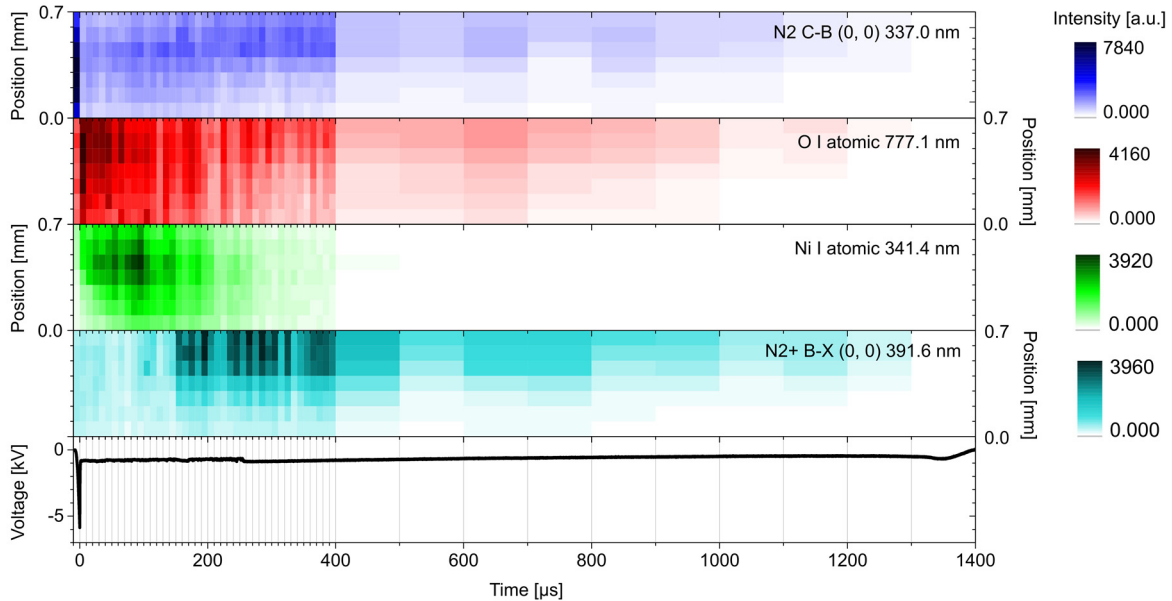


Figure 7: Spatio-temporal distribution of peak intensities of reactive species along with the secondary voltage. The y-axis of each diagram represents the spatial position from ground electrode of spark plug.

3.3 Temperature calculation process

The emission spectra, especially those of diatomic molecules like N_2 or OH, have been widely used to calculate the temperature of gas discharges [8-10] and also of hydrocarbon flames [11]. Since the electron and heavier neutral molecules are often not equally excited, the temperature of gas discharge cannot be defined simply as that of the gases in ambient condition. Commonly used terms are the electronic (T_{el}), vibrational (T_{vib}) and rotational temperature (T_{rot}) to describe electron and gas temperatures, which are not equal in most of plasma under non-equilibrium condition [12-13].

For the temperature calculation, higher spectral resolution is beneficial since the rotational structure of a diatomic molecule can be obtained. In this set of experiment, the grating with 1200 grooves/mm was selected, and the FWHM was calculated to be 0.1 nm. Two central wavelength of 355 and 385 nm were chosen: In 355 nm, N_2 C-B (0, 1) can be measured with sufficient signal-to-noise ratio, in 385 nm, both N_2 C-B and N_2^+ B-X (0, 0) can be measured.

An open-source spectrum simulation program [14] was integrated in an iteration routine. This in-house program runs the spectra simulation program with a matrix of temperatures (T_{rot} , T_{vib} , T_{el}) and generates simulated spectra. For each measured spectrum, the sum of square error was calculated to find the best fit with the least error among the matrix of simulated spectra.

3.4 Spatio-temporal variation of discharge temperature

In the analysis of following temperature estimation, a wider time step was used in order to increase signal-to-noise ratio for the calculation with less error. The data of breakdown phase was unchanged with its own 10 μs time step, but for arc and glow phase the previous time steps were merged to 100 and 200 μs respectively.

3.4.1 Rotational and vibrational temperatures – from N_2 emission at 355 nm

The rotational (T_{rot}) and vibrational temperatures (T_{vib}) of discharge were obtained by comparing measured spectra with simulated spectra at wavelength between 345 and 365 nm. In this range, N_2 C-B emission is found with two distinct peaks – vibrational band (0,1) at 357.6 nm and (1,2) at 353.6 nm [15]. Figure 8 shows samples of best-fit results from breakdown and glow discharge phases. These temperatures are also illustrated in spatio-temporally resolved style in Figure 9. The T_{rot} in breakdown phase reached only 500 K, while the temperature increased immediately from the next time step. In glow discharge phase between 600 and 1000 μs , the T_{rot} increased up to 3300 K, and the discharge cooled down slowly with time so that the T_{rot} was still about 2200 K at the very end of the discharge. The T_{vib} in breakdown phase was by far higher than T_{rot} by reaching 5000 K. In glow phase T_{vib} showed similar tendency as for T_{rot} . The temperatures obtained here in arc discharge phase between 100 and 400 K seems controversial, since the T_{vib} was calculated to be by far lower than T_{rot} [13]. The validity of this part of result will be discussed in the last section.

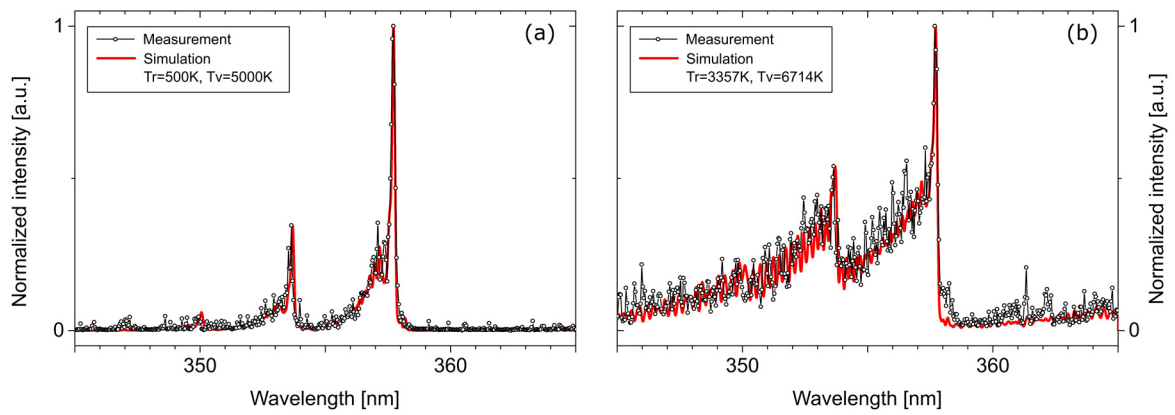


Figure 8: Best-fit results for (a) breakdown and (b) glow discharge phase for wavelength between 345 and 365 nm.

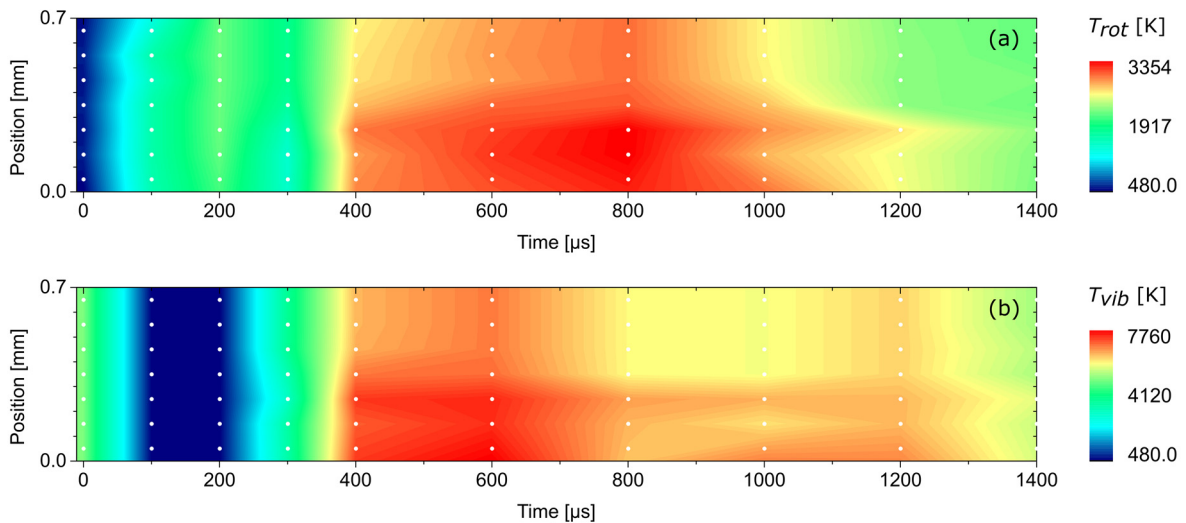


Figure 9: spatio-temporal variation of (a) rotational and (b) vibrational temperature of spark discharge.

3.4.2 Electronic temperature – from N_2 and N_2^+ emission at 385 nm

The electronic temperature (T_{el}) was obtained by comparing spectra at wavelength between 375 and 395 nm. Here, N_2 C-B emission with (0,2) band at 380.4 nm and the band head of N_2^+ B-X emission (0,0) at 391.2 nm are located. Figure 10 shows the best-fit results for breakdown and glow phase. Here, one can clearly notice the difference in the shape of spectra for two examples. The difference results from the relative intensity of N_2^+ at 391.2 nm over N_2 at 380.4 nm. The N_2^+ emission was almost negligible in breakdown phase, and as a result an extremely high T_{el} up to about 18000 K was obtained. After then, as also well illustrated in Figure 6, the N_2^+ emission increases rapidly and disappears rather slowly until the end: Oppositely, the T_e was reduced and maintained its level at around 10000 K (Figure 11).

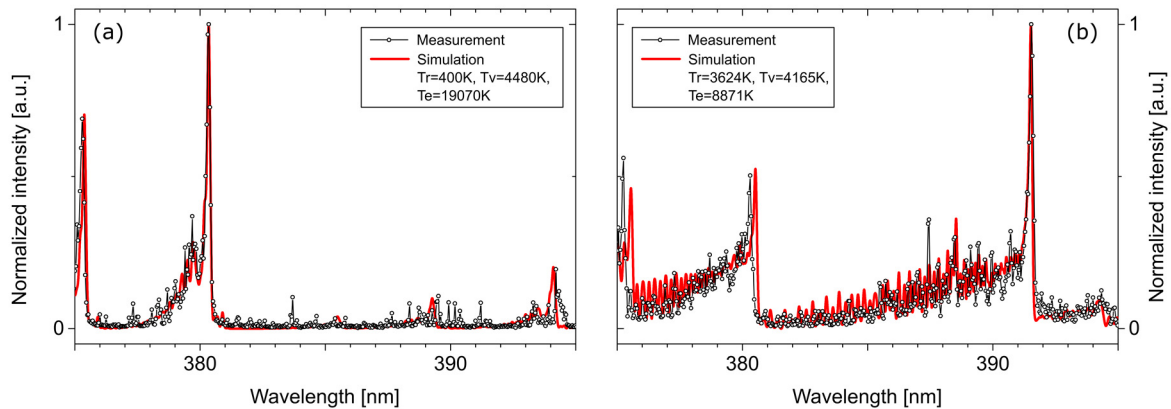


Figure 10: Best-fit results for (a) breakdown and (b) glow discharge phase for wavelength between 375 and 395 nm.

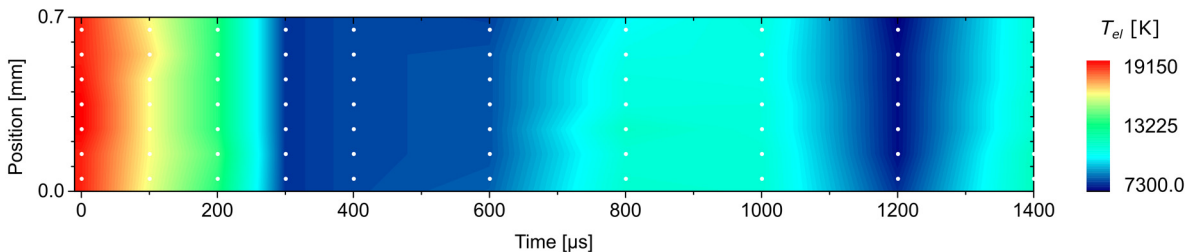


Figure 11: Spatio-temporal variation of electron temperature in spark discharge.

3.4.3 Summary with error analysis

Figure 12 illustrates the sum of square error for each best-fit results for two wavelength ranges. The darker the color of surface is, the higher the error is, i.e. the more the measured and simulated spectra deviate. Thus, it clearly indicates that the reliability of results for T_{rot} and T_{vib} is insufficient especially in the arc discharge phase between 0 and 300 μs . This verifies what caused the conflicting results discussed with Figure 9. Two reasons possibly account for this result: First, there exist numerous and intense atomic emission of nickel during arc phase, which overlap in large part with the existing N_2 emission. Second, even though there exist some measured spectra with relatively less intense Ni peaks, the N_2 emission does not show its distinct rovibrational structure. This may results either from a severely non-equilibrium state of discharge or an error induced from limited spectral resolution.

For T_e calculation, the sum of square error was globally higher than previous case, but this resulted from a wider “oscillation” of rotational structure and wavelength offset of measured spectra, as typically shown in Figure 10 between 375 and 380 nm. Looking into best-fit results individually, this can be improved by investing more computing effort with shorter and more temperature steps.

In summary, Figure 13 illustrates the spatially-averaged temporal development of T_{rot} , T_{vib} , and T_{el} of the spark discharge. The data points resulting in high sum of error are partly masked to avoid any misleading information.

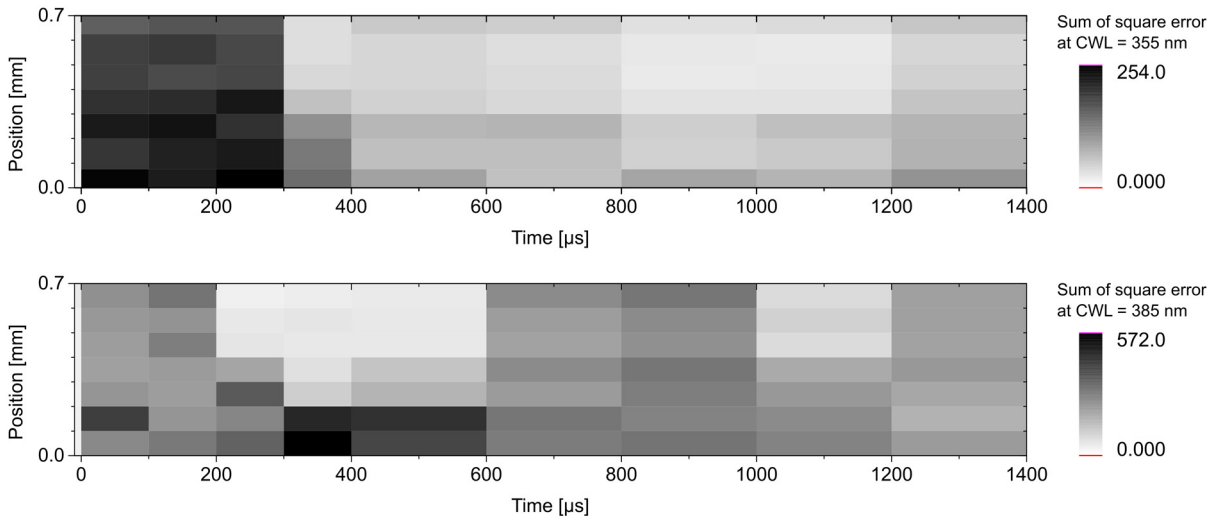


Figure 12: Sum of square error calculated from the best-fit results.

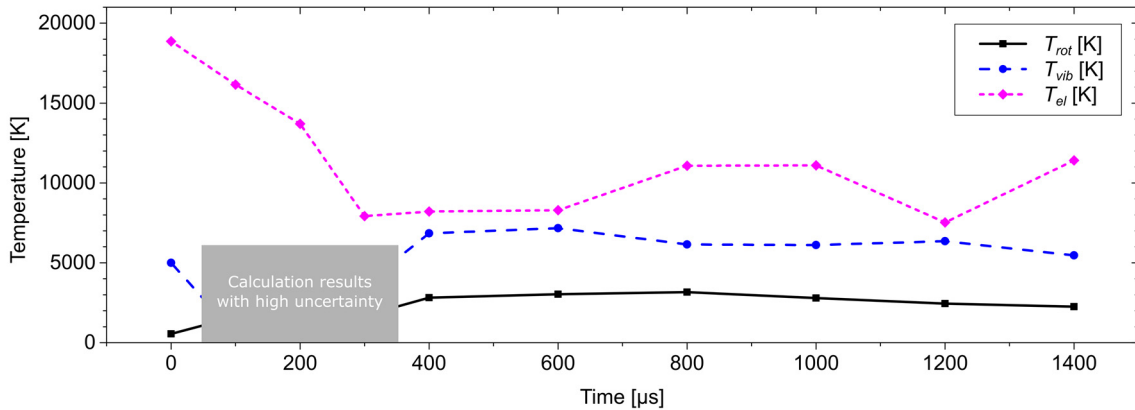


Figure 13: Temporal variation of rotational, vibrational, and electronic temperature of spark discharge.

4 Conclusions

The spark discharge of conventional automotive spark ignition system was investigated by measuring the time series of spatially-resolved emission spectra in atmospheric-pressure air condition. The experimental approach developed in this work was capable of resolving the electrode gap of spark plug in seven individual strips. The synchronization of electrical and spectroscopic measurement enabled to reconstruct the measured data into time series of information.

The major findings and remarks in this work are the following:

- The time series of peak intensity from selected reactive species showed a distinct sequence in order of N_2 –O–Ni– N_2^+ .
- The emission intensity was higher in the cathode-near region than in the anode-near region for the entire wavelength range.
- The breakdown phase showed the most intensive emission, which mainly consists of the emission from N_2 C-B transition and B-X transition. The rotational temperature (T_{rot}) of breakdown discharge was calculated to be 500 K, vibrational temperature (T_{vib}) was about 5000 K. Electronic temperature (T_{el}) reached 20000 K and was the highest during the entire spark discharge process.
- The arc discharge phase was characterized by strong atomic emission of oxygen at 777 nm followed by increase in metallic emission, in this work from nickel. The nickel atomic emission was also more intensive in cathode-near region. These emission clearly verifies the electrode wear process of spark plug.
- In the glow discharge phase the metallic emission disappears and only weak N_2 and N_2^+ B-X emission remain. The emission intensity ratio of N_2^+ to N_2 increased within the transition into glow discharge, and this had a correlation with the increase in T_{rot} up to 3000 K and decrease in T_{el} down to 10000 K. The T_{rot} was not relaxed to ambient temperature and remained to 2200K even the discharge process ended.

Acknowledgment

The authors would like to thank Leopold Seifert for the enthusiasm and effort on developing experimental setup and post-processing algorithm, and also for the constructive discussion within the research project.

References

- [1] Heywood, J. B. (1988). *Internal Combustion Engine Fundamentals*. McGraw-Hill.
- [2] Bazelyan, E. M., & Raizer, Y. P. (1997). *Spark discharge*. CRC Press.
- [3] Kim, W., Toedter, O., Koch, T., Bae, C. (2018). *Spatio-temporally resolved spectroscopic diagnostics and electrical analysis of automotive spark ignition system*. Manuscript submitted for publication.
- [4] Laux, C. O., Spence, T. G., Kruger, C. H., & Zare, R. N. (2003). Optical diagnostics of atmospheric pressure air plasmas. *Plasma Sources Science and Technology*, 12(2), 125.
- [5] Šimek, M. (2014). Optical diagnostics of streamer discharges in atmospheric gases. *Journal of Physics D: Applied Physics*, 47(46), 463001.
- [6] Sansonetti, J. E., & Martin, W. C. (2005). Handbook of basic atomic spectroscopic data. *Journal of Physical and Chemical Reference Data*, 34(4), 1559-2259.
- [7] Pearse, R. W. B., & Gaydon, A. G. (1976). *Identification of molecular spectra*. Chapman and Hall.
- [8] Moon, S. Y., & Choe, W. (2003). A comparative study of rotational temperatures using diatomic OH, O₂ and N₂⁺ molecular spectra emitted from atmospheric plasmas. *Spectrochimica Acta Part B: Atomic Spectroscopy*, 58(2), 249-257.
- [9] Nassar, H., Pellerin, S., Musiol, K., Martinie, O., Pellerin, N., & Cormier, J. M. (2004). N₂⁺/N₂ ratio and temperature measurements based on the first negative N₂⁺ and second positive N₂ overlapped molecular emission spectra. *Journal of Physics D: Applied Physics*, 37(14), 1904.
- [10] Ono, R., Nifuku, M., Fujiwara, S., Horiguchi, S., & Oda, T. (2005). Gas temperature of capacitance spark discharge in air. *Journal of applied physics*, 97(12), 123307.
- [11] Brockhinke, A., Krüger, J., Heusing, M., & Letzgus, M. (2012). Measurement and simulation of rotationally-resolved chemiluminescence spectra in flames. *Applied Physics B*, 107(3), 539-549.
- [12] Lochte-Holtgreven, W. (1968). *Plasma-diagnostics*. North-Holland Publication.
- [13] Britun, N., Gaillard, M., Ricard, A., Kim, Y. M., Kim, K. S., & Han, J. G. (2007). Determination of the vibrational, rotational and electron temperatures in N₂ and Ar–N₂ rf discharge. *Journal of Physics D: Applied Physics*, 40(4), 1022.
- [14] da Silva, M. L. (2007). An adaptive line-by-line—statistical model for fast and accurate spectral simulations in low-pressure plasmas. *Journal of Quantitative Spectroscopy and Radiative Transfer*, 108(1), 106-125.
- [15] Gilmore, F. R., Laher, R. R., & Espy, P. J. (1992). Franck–Condon factors, r-centroids, electronic transition moments, and Einstein coefficients for many nitrogen and oxygen band systems. *Journal of physical and chemical reference data*, 21(5), 1005-1107.